Errors in ultrasonic scatterer size estimates due to phase and amplitude aberration

Anthony Gerig[a] and James Zagzebski
Department of Medical Physics, University of Wisconsin—Madison, 1300 University Ave., Rm. 1530, Madison, Wisconsin 53706

(Received 16 October 2003; revised 15 March 2004; accepted 18 March 2004)

Current ultrasonic scatterer size estimation methods assume that acoustic propagation is free of distortion due to large-scale variations in medium attenuation and sound speed. However, it has been demonstrated that under certain conditions in medical applications, medium inhomogeneities can cause significant field aberrations that lead to B-mode image artifacts. These same aberrations may be responsible for errors in size estimates and parametric images of scatterer size. This work derives theoretical expressions for the error in backscatter coefficient and size estimates as a function of statistical parameters that quantify phase and amplitude aberration, assuming a Gaussian spatial autocorrelation function. Results exhibit agreement with simulations for the limited region of parameter space considered. For large values of aberration decorrelation lengths relative to aberration standard deviations, phase aberration errors appear to be minimal, while amplitude aberration errors remain significant. Implications of the results for accurate backscatter and size estimation are discussed. In particular, backscatter filters are suggested as a method for error correction. Limitations of the theory are also addressed. The approach, approximations, and assumptions used in the derivation are most appropriate when the aberrating structures are relatively large, and the region containing the inhomogeneities is offset from the insonifying transducer. © *2004 Acoustical Society of America.* [DOI: 10.1121/1.1738455]

PACS numbers: 43.80.Vj, 43.80.Qf [FD] Pages: 3244–3252

I. INTRODUCTION

The estimation and imaging of tissue parameters using ultrasound has proven to be useful in the diagnosis and monitoring of disease.[1–7] Scatterer size estimation and imaging, in particular, has been thoroughly investigated as a source of additional information beyond what is currently provided by clinical ultrasound machines.[8–12] However, the methods currently used to estimate scatterer size assume that the interrogating acoustic field is well characterized and free of distortion. They ignore aberration in the phase and amplitude of the field due to inhomogeneities located between the transducer and the region of interest. Although neglecting aberration is often appropriate and results in no significant consequences, it has been demonstrated that in certain cases, such distortion can lead to the significant deterioration of B-mode images.[13–17] Consequently, there may be instances where failing to account for aberration results in noticeable scatterer size estimation errors.

A significant amount of work has been done on the quantification of aberration, and the characterization of its effects upon ultrasonic fields. In particular, Waag *et al.* developed a theoretical scattering model which incorporates the effects of phase aberration, and relates the physical characteristics of inhomogeneities to aberration quantifiers.[18] O'Donnell looked at the effects of phase aberration upon backscatter measurement,[19] and Smith, Trahey *et al.* investigated the properties of B-mode speckle in the presence of phase aberration.[13,14] Recent work has focused primarily upon compensating for errors due to phase aberration through the incorporation of appropriate time delays in array transducer processing.[20–23] Varghese *et al.*, however, recently investigated the implications of phase aberration for elastographic imaging.[24]

In this work we extend the basic model published by Waag *et al.*[18] to include amplitude aberration due to variations in inhomogeneity attenuation with respect to the background, and investigate the effects of both aberration types (amplitude and phase) upon scatterer size estimation. In particular, aberration quantification is briefly discussed before inclusion in the general expression for Fourier-transformed rf-data segments. This expression is then used to calculate the errors in both backscatter coefficient and size estimates resulting from phase and amplitude aberration. These results are subsequently partially verified by simulations that address the two types of aberration separately. Only the limiting case, where aberration is invariant over the space occupied by an individual scatterer, is investigated. After a brief discussion of the results, possible correction filters are proposed. Finally, the limitations of the theoretical model are discussed.

II. THEORY

The following analysis closely follows the theoretical work done by Waag for phase aberration,[18] and is therefore subject to the same constraints. Namely, in order to properly apply his geometric ray/perturbation theory formalism, it must be assumed that the scale of the distorting inhomogeneities, or aberrators, are larger than the insonifying wavelength. According to Waag, the amount of phase distortion

[a]Corresponding author. Electronic mail: algerig@wisc.edu

 0001-4966/2004/115(6)/3244/9/$20.00

associated with any given point in space can be characterized by a path length correction which is associated with a phase change.[18]

$$l(\mathbf{r}) = -\int_C \gamma_c(\mathbf{r}')\, d\,\mathbf{r}', \tag{1}$$

where $\mathbf{r}$ is a point in space, γ_c is the fractional variation in sound speed at any given location from the average, c_0, and C is the straight line path from the acoustic source to the point $\mathbf{r}$, which is an approximation to the actual ray path that neglects refraction. For the sake of later analysis, the path length correction (i.e., phase aberration) will be treated as a random variable. This work will follow Waag *et al.* in assuming a zero-mean Gaussian distribution for the correction, which should be approximately valid and become moreso, according to the central limit theorem, as the number of aberrators between the source and $\mathbf{r}$ increases. In order to assure a zero-mean distribution, it will be assumed that the aberrating region is homogeneous, and that its thickness, if it does not extend throughout the entire medium, remains relatively constant across the acoustic beam.

Amplitude aberration due to attenuation variation is handled in a similar fashion. The attenuation between an acoustic source and any point in space can be expressed by

$$A(\mathbf{r},\omega) = e^{-\int_C f[\alpha(\mathbf{r}')+\alpha_0]d\,\mathbf{r}'}, \tag{2}$$

where α_0 is the average attenuation in nepers per unit distance per unit frequency, α is the deviation from this value at $\mathbf{r}'$, ω is the acoustic angular frequency, and f is the acoustic frequency. This quantity can be simplified to

$$A(\mathbf{r},\omega) = e^{-f\alpha_0|\mathbf{r}-\mathbf{r}_0|} e^{-f\psi(\mathbf{r})}, \tag{3}$$

where $\mathbf{r}_0$ is the location of the acoustic source, and

$$\psi(\mathbf{r}) = \int_C \alpha(\mathbf{r}')\, d\,\mathbf{r}'. \tag{4}$$

The first term contained in Eq. (3) is generally measured and compensated for in scatterer size estimation. In particular, the estimation method described in this work will use a point correction technique, which accounts for medium attenuation as quantified by the point approximation described below. The second term is the source of amplitude aberration, and will therefore be the focus of what follows. For the reasons mentioned previously, it will be assumed that ψ is also a zero-mean, Gaussian distributed, random variable.

In general form, the Fourier transform of a windowed ultrasonic rf data segment is given by[25]

$$V(\omega) \approx T(\omega)B(\omega)\omega^2 e^{-2f\alpha_0 z} \int_{\Delta\Omega} d\,\mathbf{r}\, \gamma(\mathbf{r}) A_t(\mathbf{r},\omega) A_r(\mathbf{r},\omega), \tag{5}$$

where aberration effects have been excluded, and gating effects have been approximated by a restriction, represented by $\Delta\Omega$, on the limits of integration over the scatterer field. The restriction includes positions in space for which $2|\mathbf{r}|/c_0$ falls within the time interval of the gate, and is most accurate when the system response for a single scatterer is short in comparison to the gate duration. $T(\omega)$ is the complex transfer function for the system transducer, $B(\omega)$ is the complex superposition coefficient corresponding to the insonifying pulse, and A_t and A_r are the field integrals for transmit and receive, respectively. $\gamma(\mathbf{r}) = [\kappa(\mathbf{r}) - \kappa_0]/\kappa_0 - [\rho(\mathbf{r}) - \rho_0]/\rho(\mathbf{r})$ is the spatially dependent reflectivity of the scattering medium, where κ and ρ are compressibility and density, and κ_0 and ρ_0 are their corresponding mean values. $e^{-2f\alpha_0 z}$ is a point approximation of the medium attenuation, where z is the distance from the transducer aperture to the point in space perpendicular to the aperture which corresponds to the middle of the time gate, and is most accurate when z is greater than the width of the active transducer aperture.[25]

To generate a size estimate for a gated segment, the Fourier transform of the segment, given by Eq. (5), is used to produce a corresponding spectral estimate. The result is divided by the magnitude squared of the appropriate point attenuation correction term and a type of system transfer function, which is, in most cases, measured using a planar reflector or reference phantom.[26,27] What remains, assuming that z is much larger than the characteristic length of the spatial autocorrelation function for the scatterers, is a backscatter estimate for the medium. This function is subsequently fit to a theoretical curve, whose frequency dependence is defined solely by scatterer size, to produce a size estimate. Several different theoretical models have been used to estimate scatterer size in tissue,[4] however, the Gaussian model for spatial autocorrelation functions will be considered exclusively here. For this case, the size estimate corresponding to an individual backscatter estimate is given by[28]

$$\hat{a}^2 = \frac{-d_1^2 c_0^2 \sum_{\omega_{\min}}^{\omega_{\max}} (y(\omega)\omega^2 - \overline{y}\,\overline{\omega^2})}{80 \sum_{\omega_{\min}}^{\omega_{\max}} (\omega^2 - \overline{\omega^2})^2}, \tag{6}$$

where $y(\omega) = 10\ln(\hat{\mathrm{BSC}}(\omega)/\omega^4)$, $d_1 \approx 3.1$ is a constant, and the summation is over discrete frequency values, correlated or uncorrelated, within the bandwidth of the transducer.

In order to discern how phase and amplitude aberration effect scatterer size estimates, aberration terms must be included in the signal equation, Eq. (5), and propagated through the mathematical machinery of size estimation described above. The resulting changes to the signal equation appear in the field integrals, and are outlined below:

$$A_{t'}(\mathbf{r},\omega) = \int_S d\,\mathbf{r}' K_t(\mathbf{r}') \frac{e^{ik|\mathbf{r}-\mathbf{r}'|}}{|\mathbf{r}-\mathbf{r}'|} e^{ikl(\mathbf{r}-\mathbf{r}')-f\psi(\mathbf{r}-\mathbf{r}')},$$

$$A_{\mathbf{r}'}(\mathbf{r},\omega) = \int_S d\,\mathbf{r}' K_r(\mathbf{r}', |\mathbf{r}-\mathbf{r}'|) \frac{e^{ik|\mathbf{r}-\mathbf{r}'|}}{|\mathbf{r}-\mathbf{r}'|} \times e^{ikl(\mathbf{r}-\mathbf{r}')-f\psi(\mathbf{r}-\mathbf{r}')}, \tag{7}$$

where the final exponential terms are the additions, S is the face of the transducer, K_t contains transmit phase and amplitude modifying terms, such as those for apodization and transmit focusing, and K_r contains analogous receive terms, including those for dynamic receive focusing, dynamic aperture, and apodization. Given these changes, the periodogram spectral estimate for a gated segment is expressed by

$$S(\omega,z)=\langle V(\omega)V^*(\omega)\rangle$$
$$=|T(\omega)B(\omega)|^2\omega^4 e^{-4f\alpha_0 z}\int\int_{\Delta\Omega} d\mathbf{r}_1\, d\mathbf{r}_2\langle \gamma(\mathbf{r}_1)\times\gamma^*(\mathbf{r}_2)\rangle\langle A_{t'}(\mathbf{r}_1,\omega)A_{r'}(\mathbf{r}_1,\omega)A^*_{t'}(\mathbf{r}_2,\omega)\times A^*_{r'}(\mathbf{r}_2,\omega)\rangle, \quad (8)$$

where it has been assumed that the aberrators and scatterers are independent, i.e. that they are not the same objects. Making the change of variable $\mathbf{r}_2=\mathbf{r}_1+\Delta\mathbf{r}$ yields

$$S(\omega,z)=|T(\omega)B(\omega)|^2\omega^4 e^{-4f\alpha_0 z}\int\int_{\Delta\Omega} d\mathbf{r}_1\, d\Delta\mathbf{r} R(\Delta\mathbf{r})\times\langle A_{t'}(\mathbf{r}_1,\omega)A_{r'}(\mathbf{r}_1,\omega)A^*_{t'}\times(\mathbf{r}_1+\Delta\mathbf{r},\omega)A^*_{r'}(\mathbf{r}_1+\Delta\mathbf{r},\omega)\rangle, \quad (9)$$

where $R(\Delta\mathbf{r})=\langle\gamma(\mathbf{r}_1)\gamma^*(\mathbf{r}_1+\Delta\mathbf{r})\rangle$ is the spatial autocorrelation function (SAF) for the scatterer field,[29] and is assumed to be statistically stationary.

Assuming that the characteristic length of the spatial autocorrelation function is small, the far-field approximation can be introduced, $k|\mathbf{r}-\mathbf{r}'+\Delta\mathbf{r}|\approx k|\mathbf{r}-\mathbf{r}'|+\mathrm{k}\cdot\Delta\mathbf{r}$ and $|\mathbf{r}-\mathbf{r}'+\Delta\mathbf{r}|\approx|\mathbf{r}-\mathbf{r}'|$, giving

$$S(\omega,z)=|T(\omega)B(\omega)|^2\omega^4 e^{-4f\alpha_0 z}\int_{\Delta\Omega} d\mathbf{r}_1 A_t(\mathbf{r}_1,\omega)\times A_r(\mathbf{r}_1,\omega)A^*_t(\mathbf{r}_1,\omega)A^*_r(\mathbf{r}_1,\omega)\times\int_{\Delta\Omega} d\Delta\mathbf{r} R(\Delta\mathbf{r})D(\mathbf{r}_1,\Delta\mathbf{r},\omega)e^{-2i\,\mathbf{k}\cdot\Delta\mathbf{r}}, \quad (10)$$

where

$$D(\mathbf{r}_1,\Delta\mathbf{r},\omega)=\langle e^{2ikl(\mathbf{r}_1)-2f\psi(\mathbf{r}_1)}e^{-2ikl(\mathbf{r}_1+\Delta\mathbf{r})-2f\psi(\mathbf{r}_1+\Delta\mathbf{r})}\rangle, \quad (11)$$

and two additional assumptions have been made. First, the direction of the vector $\mathbf{k}$ has been approximated by the direction of $\mathbf{r}_1$ rather than the true direction of $\mathbf{r}_1-\mathbf{r}'$, which is accurate given that that the distance to the gated region is larger than the size of the active area of the transducer. Second, and most importantly, it has been assumed that both forms of aberration are effectively independent of $\mathbf{r}'$, the variable of integration over the transducer surface, in order to achieve results that are both simple and field, and thus system, independent. This approximation may not always hold true, but should be acceptable when aberrator size is on the order of the transducer's active area, or the aberrating region is far from the transducer face.

If the further assumption is made that the aberration is either negligible or not present in the gated region, which is consistent with small gates or aberration due to intervening layers such as a bodywall, it follows that aberration values are invariant along the direction of the beam (approximately $\mathbf{r}_1/|\mathbf{r}_1|$) within the gated region (Fig. 1 displays the geometry for an aberrating layer). This assumption, together with the earlier homogeneity assumption, implies both that aberration variances, $\sigma_l^2(z)$ and $\sigma_\psi^2(z)$, are dependent solely upon gate position, and that correlations between aberration quantities are functions of the angular separation between their associated spatial vectors and gate position alone. For example, $\langle\psi(\mathbf{r}_1)\psi(\mathbf{r}_1+\Delta\mathbf{r})\rangle/\sigma_\psi^2(z)$ is a function of z and $\Delta\theta$, the angular separation between $\mathbf{r}_1$ and $\mathbf{r}_1+\Delta\mathbf{r}$. It therefore becomes possible to demonstrate, given the previous Gaussian distribution assumption for aberration values, that

$$D(\mathbf{r}_1,\Delta\mathbf{r},\omega)\Rightarrow D(z,\Delta\theta,\omega)=e^{4[f^2\sigma_\psi^2(z)+f^2\sigma_\psi^2(z)\rho_\psi(\Delta\theta/\theta_\psi,z)-k^2\sigma_l^2(z)+k^2\sigma_l^2(z)\rho_l(\Delta\theta/\theta_l,z)]}, \quad (12)$$

regardless of the correlation between values of l and ψ, where

$$\rho_\psi\left(\frac{\Delta\theta}{\theta_\psi},z\right)=\frac{\langle\psi(\mathbf{r}_1)\psi(\mathbf{r}_1+\Delta\mathbf{r})\rangle}{\sigma_\psi^2(z)},$$
$$\rho_l\left(\frac{\Delta\theta}{\theta_l},z\right)=\frac{\langle l\mathbf{r}_1)l(\mathbf{r}_1+\Delta\mathbf{r})\rangle}{\sigma_l^2(z)},$$

and θ_ψ and θ_l are characteristic decorrelation values similar to the decorrelation lengths of scatterer spatial autocorrelation functions. These values may be related to one another if the sources of the two types of aberration are identical, i.e., the same inhomogeneities are both phase and amplitude aberrators. If amplitude aberration is excluded, Eq. (12) is identical to the result presented by Waag *et al.* for Gaussian distributed phase aberration.[18]

Arbitrarily setting the Δz axis direction to match that of $\mathbf{r}_1$, the approximation

$$\frac{\Delta\theta}{\theta_{\psi,l}}\approx\frac{\tan\Delta\theta}{\theta_{\psi,l}}=\frac{\sqrt{\Delta x^2+\Delta y^2}}{\theta_{\psi,l}(|\mathbf{r}_1|+\Delta z)}\approx\frac{\sqrt{\Delta x^2+\Delta y^2}}{\theta_{\psi,l}|\mathbf{r}_1|} \quad (13)$$

can be used given that the integrand of Eq. (10) is suppressed by the scatterer spatial autocorrelation function for all but the smallest values of $\Delta\mathbf{r}$. Assuming a short gate and relatively narrow acoustic field such that $|\mathbf{r}_1|\approx z$, Eq. (12) can be recast:

$$D(z,\Delta\theta,\omega)\Rightarrow D(z,\omega,\sqrt{\Delta x^2+\Delta y^2})=e^{4[f^2\sigma_\psi^2(z)+f^2\sigma_\psi^2(z)\rho_\psi(\sqrt{\Delta x^2+\Delta y^2}/w_\psi)-k^2\sigma_l^2(z)+k^2\sigma_l^2(z)\rho_l(\sqrt{\Delta x^2+\Delta y^2}/w_l)]}, \quad (14)$$

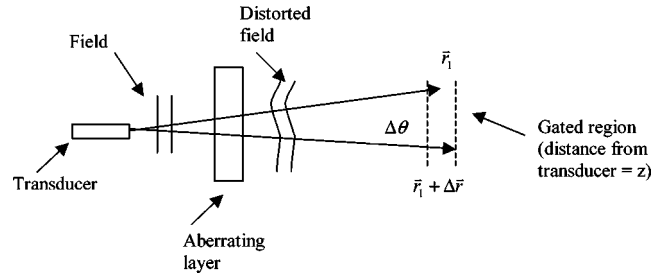

FIG. 1. Geometry for an aberrating layer. Aberration variances are independent of z for such cases as long as the gated region lies beyond the aberrating layer.

where $w_\psi = \theta_\psi z$ and $w_l = \theta_l z$ are amplitude and phase decorrelation lengths, respectively. Assuming a Gaussian form for the aberration correlation functions yields

$$D(z,\omega,\sqrt{\Delta x^2+\Delta y^2}) = e^{4[f^2\sigma_\psi^2(z)+f^2\sigma_\psi^2(z)\exp\{-(\Delta x^2+\Delta y^2)/w_\psi^2\}]} \times e^{4[-k^2\sigma_l^2(z)+k^2\sigma_l^2(z)\exp\{-(\Delta x^2+\Delta y^2)/w_l^2\}]}. \quad (15)$$

Because aberrator size must be much larger than scatterer size for the theoretical approach to be valid, the aberration decorrelation lengths must also be much larger than the characteristic length of the spatial autocorrelation function.[30] As a result, the exponential terms within the exponents of Eq. (15) will be small for nonzero values of the spatial autocorrelation function. These terms can therefore be legitimately approximated by their first-order expansions to yield

$$D(z,\omega,\sqrt{\Delta x^2+\Delta y^2}) = e^{8f^2\sigma_\psi^2-4f^2\sigma_\psi^2[(\Delta x^2+\Delta y^2)/w_\psi^2]}e^{-4k^2\sigma_l^2[(\Delta x^2+\Delta y^2)/w_l^2]}. \quad (16)$$

Using this result in Eq. (10) for a Gaussian spatial autocorrelation function, and correcting for the system response and attenuation gives

$$\langle \hat{\mathrm{BSC}}(\omega)\rangle = \mathrm{BSC}(\omega)\frac{e^{8f^2\sigma_\psi^2}}{1+2d^2/w^2}, \quad (17)$$

where d is the characteristic length of the scatterer spatial autocorrelation function, and

$$w^2 = \frac{w_\psi^2 w_l^2}{4f^2\sigma_\psi^2 w_l^2 + 4k^2\sigma_l^2 w_\psi^2}. \quad (18)$$

By inserting Eq. (17) into Eq. (6), size estimation errors can be calculated. Results are plotted in Figs. 2 and 3, where the effects of the two types of aberration have been isolated by setting the variance of the excluded type in Eq. (17) to zero. In both cases, the scatterer diameter is 80 microns, which is representative for scatterer size estimation at diagnostic frequencies, the bandwidth is 50 percent, the center frequency is set such that[9] $k_{\mathrm{cent}}a = 0.8$, and the interval between summed frequencies corresponds to the decorrelation distance for a 5 mm Hanning window. For Fig. 2, the fractional error in scatterer size is displayed as a function of w_l/σ_l, while for Fig. 3, it is plotted versus σ_ψ for several values of w_ψ, the amplitude decorrelation length. Results for lower values of the aberration decorrelation lengths should be regarded with caution given the earlier restriction that $w_{l,\psi} \gg \lambda \gg a$. As the aberration decorrelation lengths both increase and decrease, errors approach limiting values that become relatively insensitive to changes in the lengths. For example, for decreasing values of these parameters, the frequency dependence of $\langle \hat{\mathrm{BSC}}(\omega)\rangle$ approaches $\mathrm{BSC}(\omega)f^{-2}e^{8f^2\sigma_\psi^2}$, which dominates the behavior of Figs. 2 and 3 for small aberration decorrelation lengths, yet is independent of these values.

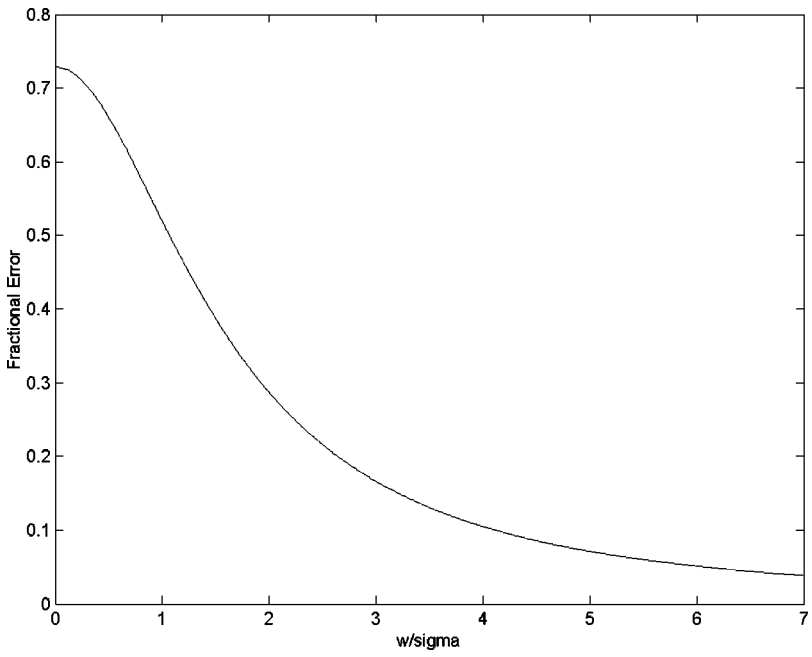

FIG. 2. Theoretical fractional error in size estimates due to phase aberration. Fractional error is plotted as a function of the ratio of phase decorrelation length to phase aberration standard deviation, w_l/σ_l.

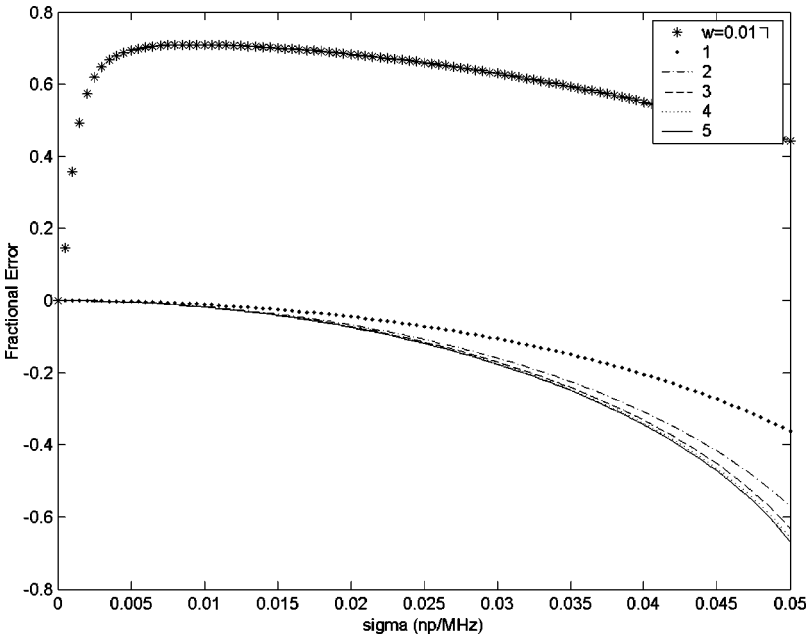

FIG. 3. Theoretical fractional error in size estimates due to amplitude aberration. Different values of amplitude decorrelation length, w_ψ (i.e., w in the legend), correspond to the different line types and are given as a fraction of scatterer radius. The fractional error is plotted as a function of amplitude aberration standard deviation, σ_ψ, which is shown in units of nepers/MHz.

III. METHOD

Verification focused upon the opposing region of parameter space where w [see Eq. (18)] is large, since, as will become evident, it can be explored without simulations that employ a high degree of complexity. Within this region, Eq. (17) can be approximated by

$$\langle \hat{\mathrm{BSC}}(\omega)\rangle \approx \mathrm{BSC}(\omega) e^{8f^2\sigma_\psi^2}, \tag{19}$$

which indicates that while amplitude aberration remains a source of error, phase aberration does not. This result is equivalent to what is obtained when it is assumed that aberration values are effectively invariant over the characteristic length of the spatial autocorrelation function. Under this assumption, the correlation functions of Eq. (12) can be replaced by unity, leaving a quantity that can be extracted from the integrals of Eq. (10) to yield an expression that reduces to Eq. (19).

Simulated rf data were generated using code[31] that artificially implements a Gaussian spatial autocorrelation function by multiplying the frequency-dependent scattered amplitude from randomly distributed point-like scatterers by the square root of the form factor for a Gaussian spatial autocorrelation function, $e^{-k^2d^2}$. Typically, such an implementation would be inadequate for studying aberration effects since it cannot incorporate effects due to changing aberration values over the dimension of a spatially extended scatterer. However, because size estimate errors in the region of parameter space under consideration are equivalent to those obtained under the assumption of aberration invariance on the scale of scatterer size as described above, it can be appropriately used. Aberration effects were included by multiplying the frequency dependent scattered amplitude for each scatterer by either

$$e^{-2f\sigma_\psi(z)n} \quad \text{or} \quad e^{2ik\sigma_l(z)n}, \tag{20}$$

for amplitude and phase aberration respectively, where n is a random number drawn from a zero-mean, unity-standard deviation Gaussian probability distribution.

Several independent planes of rf data (300 acoustic lines per plane) were generated for a simulated linear array transducer (0.15 mm by 10 mm elements with 0.2 mm spacing; 5 cm transmit and elevational foci; 10 elements active during transmit; dynamic receive focus, dynamic aperture, and apodization active). In all cases, the average speed of sound was set to 1540 m/s, the average attenuation to 0, the scatterer density to 4000 per cubic cm, the transducer center frequency to 7 MHz, and the bandwidth to 5.5 MHz. The sampling frequency was set by the code to be approximately 38 MHz. 17 aberration-free reference planes were generated for backscatter estimation, where the scatterer diameter was 50 microns. Planes that included aberration were generated in sets of two across multiple values of aberration variance. Each set incorporated only one type of aberration, and all scatterer diameters were 75 microns. Backscatter estimates were produced for each of the 300 acoustic lines using the reference phantom method,[27] where the necessary power spectral estimates were drawn from 1 cm data segments centered about a depth of 4 cm. Sample power spectral estimates were averaged across each 2-plane set, and reference power spectral estimates across all 17 planes. The results were used to generate size estimates using the method described previously. The fractional error was calculated for each size estimate, and mean and standard deviation point estimates of the fractional error were produced for each value of aberration variance.

IV. RESULTS

Figures 4 and 5 display the results for phase and amplitude aberration, respectively. In both cases, the mean fractional error is plotted as a function of the aberration standard deviation. Error bars correspond to the approximate standard error of the mean, and theoretical values were generated nu-

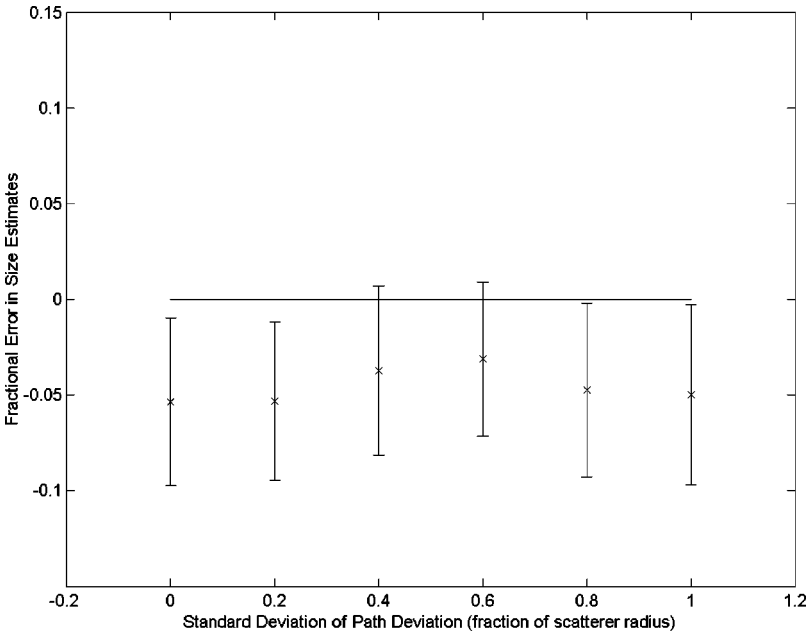

FIG. 4. A comparison of theoretical and simulation size estimate fractional errors as a function of path deviation (i.e., phase aberration) standard deviation when the phase decorrelation length is much larger than the phase aberration standard deviation.

merically according to Eqs. (19) and (6). All values, including the phase aberration control, are biased low. This error appears to be the result of an inherent bias in the backscatter coefficient estimation technique, although bias in the size estimator could also be a contributing factor. The more noise contained in the reference spectral estimate, the worse the bias of the reference phantom method. Otherwise, the agreement between simulation and theoretical values appears to be good.

V. DISCUSSION

According to the results contained in Fig. 4, phase aberration should have a minimal effect upon size estimates for typical values of the phase decorrelation length unless the aberration standard deviation is high. As a result, corrections should only be necessary under this condition, given that the stated assumptions of the theoretical section hold. Figure 5, on the other hand, indicates that amplitude aberration can cause significant errors for modest values of aberration standard deviation, regardless of the value of the amplitude decorrelation length. Errors, in fact, appear to be maximal for larger values of the decorrelation length. However, the form of Eqs. (17) and (19) suggests a relatively simple method to correct for amplitude aberration. Assuming that σ_ψ is known and that w_ψ, the amplitude decorrelation length, is comparatively large, the filter

$$H(\omega) = e^{-8f^2\sigma_\psi^2}, \tag{21}$$

can be applied to backscatter estimates before size estimation to effectively eradicate any detrimental aberration effects. Notice that according to Eqs. (17) and (18), the filter can be

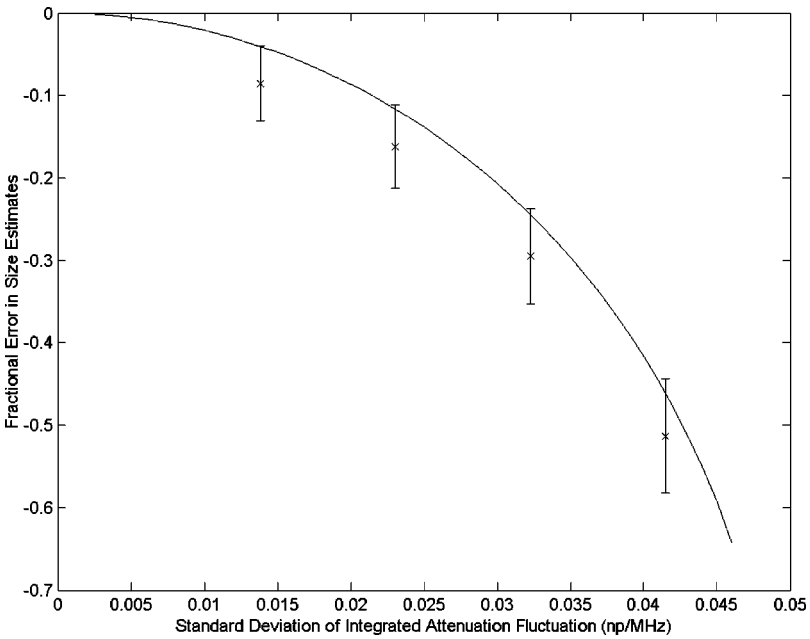

FIG. 5. A comparison of theoretical and simulation size estimate fractional errors caused by amplitude aberration when the amplitude decorrelation length is much greater than the amplitude aberration standard deviation. Fractional error is plotted as a function of amplitude aberration standard deviation in units of nepers/MHz.

adapted to account for both amplitude and phase aberration when aberration standard deviations are higher. However, an approximate *a priori* knowledge of scatterer size and aberration decorrelation lengths is necessary in order to make the appropriate adjustments.

Although the effects of phase and amplitude aberration upon size estimation have been adequately characterized under the stated restrictions, the assumption that both forms of aberration are independent of $\mathbf{r}'$, which was made in order to arrive at Eqs. (10) and (11), excludes aberration due to moderately sized inhomogeneities close to the active face of the transducer. If this assumption is withdrawn, the expected value of Eq. (9), rather than simplifying to the form found in Eq. (10), becomes

$$\int_{S^{(1)}}\int_{S^{(2)}}\int_{S^{(3)}}\int_{S^{(4)}} K_t(\mathbf{r}^{(1)})K_{\mathbf{r}}(\mathbf{r}^{(2)},|\mathbf{r}_1-\mathbf{r}^{(2)}|)K_t^*(\mathbf{r}^{(3)})K_r^*(\mathbf{r}^{(4)},|\mathbf{r}_1+\Delta\,\mathbf{r}-\mathbf{r}^{(4)}|)$$
$$\times\frac{e^{ik|\mathbf{r}_1-\mathbf{r}^{(1)}|}e^{ik|\mathbf{r}_1-\mathbf{r}^{(2)}|}e^{-ik|\mathbf{r}_1+\Delta\,\mathbf{r}-\mathbf{r}^{(3)}|}e^{-ik|\mathbf{r}_1+\Delta\,\mathbf{r}-\mathbf{r}^{(4)}|}}{|\mathbf{r}_1-\mathbf{r}^{(1)}||\mathbf{r}_1-\mathbf{r}^{(2)}||\mathbf{r}_1+\Delta\,\mathbf{r}-\mathbf{r}^{(3)}||\mathbf{r}_1+\Delta\,\mathbf{r}-\mathbf{r}^{(4)}|}\langle e^{ikl(\mathbf{r}_1-\mathbf{r}^{(1)})-f\psi(\mathbf{r}_1-\mathbf{r}^{(1)})}e^{ikl(\mathbf{r}_1-\mathbf{r}^{(2)})-f\psi(\mathbf{r}_1-\mathbf{r}^{(2)})}$$
$$\times e^{-ikl(\mathbf{r}_1+\Delta\,\mathbf{r}-\mathbf{r}^{(3)})-f\psi(\mathbf{r}_1+\Delta\,\mathbf{r}-\mathbf{r}^{(3)})}e^{-ikl(\mathbf{r}_1+\Delta\,\mathbf{r}-\mathbf{r}^{(4)})-f\psi(\mathbf{r}_1+\Delta\,\mathbf{r}-\mathbf{r}^{(4)})}\rangle. \tag{22}$$

Not only is this expression extremely complex, but it also implies that backscatter and size estimation errors will be field dependent, given that the aberration term is a function of the field integration variables. As a result, characterization of the error will be both difficult and system specific. The one case that is easily calculable is the limit where the correlation between aberration values approaches zero, such that

$$\langle e^{ikl(\mathbf{r}_1-\mathbf{r}^{(1)})-f\psi(\mathbf{r}_1-\mathbf{r}^{(1)})}e^{ikl(\mathbf{r}_1-\mathbf{r}^{(2)})-f\psi(\mathbf{r}_1-\mathbf{r}^{(2)})}e^{-ikl(\mathbf{r}_1+\Delta\,\mathbf{r}-\mathbf{r}^{(3)})-f\psi(\mathbf{r}_1+\Delta\,\mathbf{r}-\mathbf{r}^{(3)})}e^{-ikl(\mathbf{r}_1+\Delta\,\mathbf{r}-\mathbf{r}^{(4)})-f\psi(\mathbf{r}_1+\Delta\,\mathbf{r}-\mathbf{r}^{(4)})}\rangle$$
$$\approx\langle e^{ikl(\mathbf{r}_1-\mathbf{r}^{(1)})-f\psi(\mathbf{r}_1-\mathbf{r}^{(1)})}\rangle\langle e^{ikl(\mathbf{r}_1-\mathbf{r}^{(2)})-f\psi(\mathbf{r}_1-\mathbf{r}^{(2)})}\rangle\langle e^{-ikl(\mathbf{r}_1+\Delta\,\mathbf{r}-\mathbf{r}^{(3)})-f\psi(\mathbf{r}_1+\Delta\,\mathbf{r}-\mathbf{r}^{(3)})}\rangle\langle e^{-ikl(\mathbf{r}_1+\Delta\,\mathbf{r}-\mathbf{r}^{(4)})-f\psi(\mathbf{r}_1+\Delta\,\mathbf{r}-\mathbf{r}^{(4)})}\rangle$$
$$=e^{2\,f^2\sigma_\psi^2-2k^2\sigma_l^2}. \tag{23}$$

Because this result is independent of all integration variables, given the previous assumptions of the theoretical section, its associated backscatter error can be obtained immediately:

$$\langle\hat{\mathrm{BSC}}(\omega)\rangle=\mathrm{BSC}(\omega)e^{2\,f^2\sigma_\psi^2-2k^2\sigma_l^2}. \tag{24}$$

However, for this limit to be remotely applicable to physical cases, aberrating inhomogeneities must be small in comparison to the active area of the transducer, a condition which may rarely be met by objects which must also meet a minimum size requirement for the theory to be accurate.

VI. CONCLUSION

Expressions for the errors in ultrasonic backscatter coefficient and size estimates due to phase and amplitude aberration were derived based upon the theoretical framework described by Waag *et al.*[18] For large values of aberration decorrelation lengths relative to aberration standard deviations, theoretical results compared favorably with simulations. Under these conditions, phase aberration errors appear to be minimal, while amplitude aberration errors remain significant. However, a simple filter can be applied to backscatter estimates, assuming that the amplitude aberration variance is known to correct for the error. When aberration standard deviations are comparatively large, the filter can be modified to correct for higher order phase and amplitude aberration given that prior knowledge of the approximate scatterer size and aberration decorrelation lengths is available.

Although the results of the aberration error characterization are relatively simple, their applicability is somewhat limited by the assumptions that were made in their derivation. Namely, they are accurate only in cases where the aberrating inhomogeneities are large in comparison to and/or distant from the insonifying transducer.

ACKNOWLEDGMENTS

This work was supported in part by NIH Grants No. R01CA39224, No. R21EB002722, and No. T32CA09206.

TABLE OF SYMBOLS

A	attenuation between an acoustic source and a point in space
A_r	receive acoustic field integral
$A_{r'}$	receive acoustic field integral including aberration effects
A_t	transmit acoustic field integral
$A_{t'}$	transmit acoustic field integral including aberration effects
a	scatterer size (radius)
$\hat{a}$	scatterer size estimate (radius)
α_0	average attenuation for a medium
α	deviation from the average attenuation at a point in space
B	complex superposition coefficient corresponding to an insonifying pulse
BSC	backscatter coefficient
$\hat{\mathrm{BSC}}$	backscatter coefficient estimate

C	straight line path from an acoustic source to a spatial point
c_0	average speed of sound for a medium
d	characteristic length of a scatterer spatial autocorrelation function
d_1	a constant
$\Delta\Omega$	spatial approximation of a temporal gate
$\Delta\theta$	angular separation between spatial vectors
f	acoustic frequency
γ_c	fractional variation in sound speed from the average
γ	reflectivity
H	aberration correction filter
$k,\mathbf{k}$	acoustic wave number
k_{cent}	wave number corresponding to a transducer center frequency
κ	compressibility
κ_0	average compressibility for a medium
K_r	signal processing term included in the receive acoustic field integral
K_t	signal processing term included in the transmit acoustic field integral
l	path length correction associated with phase aberration
λ	acoustic wavelength
n	random variable
ρ	mass density
ρ_0	average mass density for a medium
ρ_l	phase aberration correlation
ρ_ψ	amplitude aberration correlation
ψ	integrated (along the path from transducer to scatterers) deviation from the average attenuation
$\mathbf{r},\mathbf{r}',\mathbf{r}_0$	spatial variables/vectors
$\mathbf{r}_1,\mathbf{r}_2,\Delta\mathbf{r},\mathbf{r}^{(n)}$	
R	spatial autocorrelation function (SAF) for a scatterer field
S	transducer surface periodogram spectral estimate
σ_l^2	phase aberration variance
σ_ψ^2	amplitude aberration variance
T	the complex transfer function for a system transducer
θ_l	phase aberration decorrelation angle
θ_ψ	amplitude aberration decorrelation angle
V	Fourier transform of a windowed ultrasonic rf data segment
w	a combination of aberration decorrelation lengths and variances
w_l	phase aberration decorrelation length
w_ψ	amplitude aberration decorrelation length
ω	acoustic angular frequency
$\omega_{\min}$	lower limit of transducer bandwidth
$\omega_{\max}$	upper limit of transducer bandwidth
y	transformed backscatter coefficient estimate
z	perpendicular distance from a transducer aperture to the middle of a gated region

[1] S. L. Bridal, P. Fornes, P. Bruneval, and G. Berger, "Parametric (integrated backscatter and attenuation) images constructed using backscattered radio frequency signals (25–56 MHz) from human aortae in vitro," Ultrasound Med. Biol. **23**, 215–229 (1997).

[2] E. J. Feleppa, F. L. Lizzi, D. J. Coleman, and M. M. Yaremko, "Diagnostic spectrum analysis in ophthalmology: A physical perspective," Ultrasound Med. Biol. **12**, 623–631 (1986).

[3] M. Insana and T. Hall, "Parametric ultrasound imaging from backscatter coefficient measurements: Image formation and interpretation," Ultrason. Imaging **12**, 245–267 (1990).

[4] M. Insana, R. Wagner, D. Brown, and T. Hall, "Describing small-scale structure in random media using pulse-echo ultrasound," J. Acoust. Soc. Am. **87**, 179–192 (1990).

[5] R. Kuc and M. Schwartz, "Estimating the acoustic attenuation coefficient slope for liver from reflected ultrasound signals," IEEE Trans. Sonics Ultrason. **26**, 353–362 (1979).

[6] F. Lizzi, M. Ostromogilsky, E. Feleppa, M. Rorke, and M. Yaremko, "Relationship of ultrasonic spectral parameters to features of tissue microstructure," IEEE Trans. Ultrason. Ferroelectr. Freq. Control **34**, 319–328 (1987).

[7] P. Stetson and G. Sommer, "Ultrasonic characterization of tissues via backscatter frequency dependence," Ultrasound Med. Biol. **23**, 989–996 (1997).

[8] T. Hall, M. Insana, L. Harrison, and G. Cox, "Ultrasonic measurement of glomerular diameters in normal adult humans," Ultrasound Med. Biol. **22**, 987–997 (1996).

[9] M. Insana and T. Hall, "Characterising the microstructure of random media using ultrasound," Phys. Med. Biol. **35**, 1373–1386 (1990).

[10] M. Insana, T. Hall, J. Wood, and Z.-y. Yan, "Renal ultrasound using parametric imaging techniques to detect changes in microstructure and function," Invest. Radiol. **28**, 720–725 (1993).

[11] M. L. Oelze, J. F. Zachary, and J. William D. O'Brien, "Parametric imaging of rat mammary tumors *in vivo* for the purposes of tissue characterization," J. Ultrasound Med. **21**, 1201–1210 (2002).

[12] R. L. Romijn, J. M. Thijssen, and G. W. J. V. Beuningen, "Estimation of scatterer size from backscattered ultrasound: A simulation study," IEEE Trans. Ultrason. Ferroelectr. Freq. Control **36**, 593–606 (1989).

[13] S. W. Smith, G. E. Trahey, and S. M. Hubbard, "Properties of acoustical speckle in the presence of phase aberration Part II: Correlation lengths," Ultrason. Imaging **10**, 29–51 (1988).

[14] G. E. Trahey and S. W. Smith, "Properties of acoustical speckle in the presence of phase aberration Part 1: First order statistics," Ultrason. Imaging **10**, 12–28 (1988).

[15] W. A. Smith, R. C. Waag, and D. Dalecki, Assessing the limits of ultrasonic focusing through tissue from scattering measurements, *Ultrasonics Symposium* (IEEE, Chicago, 1988), pp. 809–814.

[16] L. M. Hinkelman, T. D. Mast, L. A. Metlay, and R. C. Waag, "The effect of abdominal wall morphology on ultrasonic pulse distortion. Part 1. Measurements," J. Acoust. Soc. Am. **104**, 3635–3650 (1998).

[17] T. D. Mast, L. M. Hinkelman, M. J. Orr, and R. C. Waag, "The effect of abdominal wall morphology on ultrasonic pulse distortion. Part II. Simulations," J. Acoust. Soc. Am. **104**, 3651–3664 (1998).

[18] R. C. Waag, J. P. Astheimer, and G. W. Swarthout, "A characterization of wavefront distortion for analysis of ultrasound diffraction measurements made through an inhomogeneous medium," IEEE Trans. Sonics Ultrason. **32**, 36–48 (1985).

[19] M. O'Donnell, "Quantitative ultrasonic backscatter measurements in the presence of phase distortion," J. Acoust. Soc. Am. **72**, 1719–1725 (1982).

[20] S. W. Flax and M. O'Donnell, "Phase-aberration correction using signals from point reflectors and diffuse scatterers: Basic principles," IEEE Trans. Ultrason. Ferroelectr. Freq. Control **35**, 758–767 (1988).

[21] M. O'Donnell and S. W. Flax, "Phase-aberration correction using signals from point reflectors and diffuse scatterers: Measurements," IEEE Trans. Ultrason. Ferroelectr. Freq. Control **35**, 768–774 (1988).

[22] S. Krishnan, P.-C. Li, and M. O'Donnell, "Adaptive compensation of phase and magnitude aberrations," IEEE Trans. Ultrason. Ferroelectr. Freq. Control **43**, 44–55 (1996).

[23] D.-L. Liu and R. C. Waag, "Estimation and correction of ultrasonic wavefront distortion using pulse-echo data received in a two-dimensional aperture," IEEE Trans. Ultrason. Ferroelectr. Freq. Control **45**, 473–489 (1998).

[24] T. Varghese, M. Bilgen, and J. Ophir, "Phase aberration effects in elastography," Ultrasound Med. Biol. **27**, 819–827 (2001).

[25] J.-F. Chen, J. Zagzebski, F. Dong, and E. Madsen, "Estimating the spatial autocorrelation function for ultrasound scatterers in isotropic media," Med. Phys. **25**, 648–655 (1998).

[26] E. L. Madsen, M. F. Insana, and J. A. Zagzebski, ''Method of data reduction for accurate determination of acoustic backscatter coefficients,'' J. Acoust. Soc. Am. **76**, 913–923 (1984).
[27] L. X. Yao, J. A. Zagzebski, and E. L. Madsen, ''Backscatter coefficient measurements using a reference phantom to extract depth-dependent instrumentation factors,'' Ultrason. Imaging **12**, 58–70 (1990).
[28] A. Gerig, J. Zagzebski, and T. Varghese, ''Statistics of ultrasonic scatterer size estimation with a reference phantom,'' J. Acoust. Soc. Am. **113**, 3430–3437 (2003).
[29] M. Insana and D. Brown, ''Acoustic scattering theory applied to soft biological tissues,'' in *Ultrasonic Scattering in Biological Tissues*, edited by K. Shung (CRC Press, Boca Raton, FL, 1993), pp. 75–124.
[30] R. C. Waag and D. Dalecki, ''Estimates of wavefront distortion from measurements of scattering by model random media and calf liver,'' J. Acoust. Soc. Am. **85**, 406–415 (1988).
[31] Y. Li and J. A. Zagzebski, ''A frequency domain model for generating B-mode images with array transducers,'' IEEE Trans. Ultrason. Ferroelectr. Freq. Control **46**, 690–699 (1999).